Digest Journal of Nanomaterials and Biostructures Vol. 11, No. 2, April - June 2016, p. 411 - 418

ABSENCE OF ROOM TEMPERATURE FERROMAGNETISM IN Co AND Cr CO-DOPED TiO_2 BASED DILUTE MAGNETIC SEMICONDUCTORS

S. WASEEM*, S. ANJUM, L. MUSTAFA, T. ZEESHAN, R. ZIA, N. MOHSIN
Department of Physics, Lahore College for Women University, Lahore 54000, Pakistan

Co and Cr Co-doped Titanium Dioxide, $Ti_{0.9}Cr._{1-x}Co_xO_2$ (x=0.0, 0.02, 0.04, 0.06, 0.08 and .10), Dilute magnetic semiconductors (DMSs) were synthesized by solid state reaction method at annealing temperature of 1050^0C for six hours. XRD patterns confirmed the single phase rutile. The rutile structure was also confirmed by Raman spectroscopy technique. Grain sizes were measured by Scanning Electron Microscope (SEM). The samples were examined for its magnetic property using Vibrating Sample Magnetometer (VSM) at room temperature which indicated Paramagnetic behavior. Electrical resistivity as a function of temperature was measured using four probe technique. Band gap energy was calculated by UV Visible spectroscopy. Both electrical resistivity measurements and band gap measurements confirmed the semiconducting nature of $Ti_{0.9}Cr._{1-x}Co_xO_2$ series.

(Received February 1, 2016; Accepted April 15, 2016)

Keywords: Dilute magnetic semiconductors, Rutile, TiO_2, Tetragonal, Paramagnetic

1. Introduction

Dilute magnetic semiconductors (DMS) have the properties of both semiconductors and magnetic materials [1].They consist of semiconducting material doped with a few atomic percent of magnetic cation i.e. transition metals [2]. 3d transition metals like Fe, Co, and Ni, have partially filled d states. These partially filled d states contain unpaired electrons and responsible for exhibiting magnetic behavior. The addition of 3d transition metal ions can change the Fermi energy state by raising the valance band maximum and lowering the conduction band minimum, thus reducing the band gap [3]. Initial trials to observe ferromagnetism was carried out in II-VI and III-V semiconducting materials, such as Mn doped CdTe and Mn doped GaAs, etc .Although Ohno achieved ferromagnetism in Mn doped GaAs, the Curie temperature (T_c) was very less (T_c=110 K). Initial attempt on oxide based DMS was started by Matsumoto et al. in Co doped TiO_2 thin film, prepared by combinatorial pulsed-laser deposition (PLD) molecular-beam epitaxy (MBE), and obtained a T_c well above room temperature [4]. Among oxide based (O-DMSs) Titanium dioxide (TiO_2) presents interesting properties such as transparent to visible light absorption, has a wide band gap, high refractive index and low absorption. These properties are promising for applications as catalysts, Photo anodes, Solar cells, magneto-optical applications [5]. TiO_2 doped with Cobalt or Iron displays room temperature ferromagnetism both in Anatase and Rutile forms for different dopant concentrations. The magnetic behavior at room temperature varies largely with the fabrication method and growth conditions [6]. However the mechanism of magnetic ordering at room temperature is under discussion and is not understood still [7]. Among transition metal doped Cr is an important dopant both theoretically and experimentally as it has a major effect on carrier mobility. It appears to be ferromagnetic dopant in thin films [8].

A lot of work has been done on TiO_2 based DMS with doping of single transition metal but a little attention has been paid on co-dopants. Co-doping can lead to remarkable improvement in properties of DMS. Chakrabari et al reported that saturation magnetic field can be enhanced by adding 2% of Fe in Co-ZnO system [9, 10].

* Corresponding author: salma_iqbal1990@hotmail.com

The present work is an experimental one in which Co and Cr have been used as co-dopants in TiO_2 .The purpose of Co- doping is to induce the room temperature ferromagnetism and to enhance charge carrier density in TiO_2. As a result the magnetic and electrical properties may be enhanced which would improve its efficiency for DMS applications.

2. Experimentation

A series of six powder samples having general formula $Ti_{0.9}\ Co._{1-x}Cr_xO_2$ (x= 0.00, 0.02, 0.04, 0.06, 0.08 and 0.10) has been prepared by Powder metallurgy route. All the samples have been weighed according to their stoichiometric ratio by using a precise electronic balance. After weighing all the powder samples have been mixed and grinded individually by using Ceramic Mortar and Pestle to get homogenous mixture. These raw samples are then annealed in heating furnace at 1050^oC for 6 hours. Some of material of prepared samples is used to make pallets for electrical resistivity measurement. Carver pallet press is used to make disc shaped pallets of 1.3 mm diameter with acetone as a binder. The prepared pallets are then heated at 650 ^oC for 2 hours just for the purpose of hardening.

In this work Crystal structure and phase identification of the samples have been examined using X-ray diffractometer D-8 discover, Bruker, made in Germany, having source Cu-K_α radiations with the wavelength λ = 1.540598 Å. UV-Visible analysis has been done to study the variation of band gap. The samples have been examined optically by using UV 2800 model, Hitachi Japan, having wavelength 300 to 900 nm. Surface morphology of the samples has been observed through scanning electron microscope (SEM) using S-3400N Hitachi. Room temperature Magnetic measurements are performed by Lakeshore 7436 vibrating sample magnetometer. Electrical resistivity measurements have been carried out by four probe technique at varying temperature.

3. Results and discussion

3.1 XRD ANALYSIS

The Comparative XRD patterns of series having general formula $Ti_{0.9}Co_{0.1-x}Cr_xO_2$ (x=0, 0.02, 0.04, 0.06, 0.08 and 0.10) are shown in Fig.1. All peaks have been matched with JCPDS card number 21-1276 which has confirmed the rutile structure, i.e. tetragonal structure. There are some minor peaks of Ti_2O_3 with value of x= 0.0, 0.02, 0.04 at 2θ= 32.95 respectively. However these peaks vanished at x= 0.06, 0.08 and 0.1 respectively and a true rutile Phase is developed. From these XRD micrographs, the most intense diffraction peak has been selected and lattice constants a and c are determined by the following relation [2].

$$\frac{1}{d^2} = \frac{h^2+k^2}{a^2} + \frac{l^2}{c^2} \qquad (1)$$

Where d is the interplanar distance and hkl are the miller indices of corresponding plane. It is observed that as the concentration of Cr increases the values of lattice constants 'a' and 'c' increase. This is due to the fact Cr^{2+} ions have large ionic radius (0.87A°) compared to Ti^{+4} (0.68A°) and Co^{2+} (0.58A°). As the divalent Cr ions are substituted for metallic ions in the lattice, the Cr content replaces smaller Ti^{+4} ions elongating the lattice [10, 11, 12, and 13]. Average crystalline size is calculated by Sherrer's formula which is given below.

$$D = k\,\lambda / \beta\,\mathrm{Cos}\theta \qquad (2)$$

Where k is a constant having value 0.94. λ is wavelength of Cu-K_α .It's value is 0 .54×10-10 m , β is full width at half maximum. The values of crystallite size (D), lattice constants 'a' and 'c' with varying concentration of x are given in Table 1.

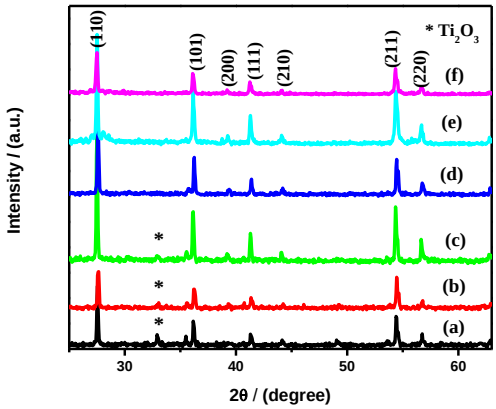

Fig 1. Comparative XRD patterns of $Ti_{0.9}Co_{0.1-x}Cr_xO_2$ (x=a=0.0, x=b=0.02, x=c=0.04, x=d=0.06, x=e=0.08, x=f=0.1)

Table1. Values of crystallite size, lattice constants, grain size and band gap energy of $Ti_{0.9}Co_{0.1-x}Cr_xO_2$ (x=0.0, 0.02, 0.04, 0.06, 0.08, 0.1)

Cr Conc. /x	D/nm	a/nm	c/nm	Grain Size / µm	Eg /eV
0.0	95.297	0.4560	0.293	3.1	2.82
0.02	95.289	0.4562	0.293	2.9	2.72
0.04	95.287	0.4562	0.294	2.7	2.72
0.06	95.276	0.4573	0.294	2.5	2.52
0.08	53.276	0.4579	0.295	2.4	2.52
0.1	51.275	0.4582	0.296	2.1	2.5

3.2 Raman spectroscopy analysis

Raman spectra of the series $Ti_{0.9}Co_{0.1-x}Cr_xO_2$ (x=0.0, 0.02, 0.04, 0.06, 0.08, 0.1) is shown in Fig.2. The rutile phase exhibits major peaks at 610, 446, and 242 cm^{-1} and minor peaks at 818, 707, and 319 cm^{-1}[14]. From the spectra it is observed that there are three major peaks present i.e. at 264, 415 and 608 cm^{-1} and two minor peaks at 315 and 706 cm^{-1} respectively. Usually the four active Raman vibration modes of rutile phase are given

$$A_{1g} + B_{1g} + B_{2g} + Eg \quad (3)$$

The peak at 415cm^{-1} and 608 cm^{-1} belong to E_g and A_{1g} mode respectively whereas the peak at 264 $cm^{-1}$is known as compound vibration peak due to multiple phonon scattering process .This peak is also known as Characteristic Raman peak of rutile TiO_2 [15,16,17]. The peak corresponding to B_{1g} i.e. at 143 cm^{-1} is not observed due to technical limitations of the Raman device. There is a slight Raman shift in observed values because of mixing of dopants having different sizes of ionic radii with increased concentration of Cr. Moreover, Lattice strain, defects, and crystallite size have a profound effect in the shifting, peak broadening and on the intensity of the Raman peak.

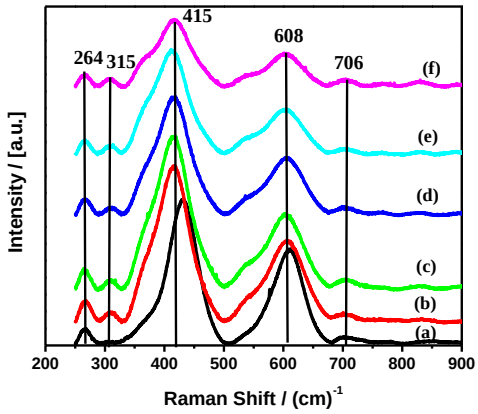

Fig 2. Comparative Raman spectra of $Ti_{0.9}Co_{0.1-x}Cr_xO_2$ (x=a=0.0, x=b=0.02, x=c=0.04, x=d=0.06, x=e=0.08, x=f=0.1)

3.3 FTIR Analysis

FTIR spectra of the series $Ti_{0.9}Co_{0.1-x}Cr_xO_2$ (x=0.0, 0.02, 0.04, 0.06, 0.08, 0.1) is shown in Fig.3. From the FTIR spectra different vibration bands can be observed. The broad band below 1000 cm^{-1} (having minima at 722,590, 525, and 471 cm^{-1}) can be attributed to characteristic Ti–O and Ti–O–Ti stretching and bending vibrational modes for rutile TiO_2 [16] .The weak band around 1000 cm^{-1} is due to the ionic character of Ti-O bonds [18].The absorption band at 1400 cm^{-1} is due to CO_2 in air. It might be formed due to burning gases inside the furnace during heating of powder samples [19]. The peak at 1651 cm^{-1} is due to water molecules in KBr, which has been used in the preparation of samples for FTIR analysis. A small absorption peak observed around 2436–2438cm^{-1} is due to the existence of CO_2 molecule in air. [20]

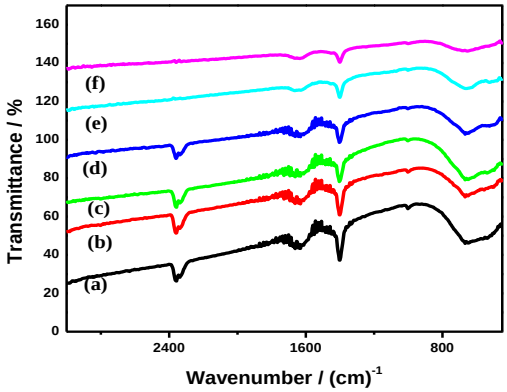

Fig 3. Comparative FTIR spectra of $Ti_{0.9}Co_{0.1-x}Cr_xO_2$ (x=a=0.0, x=b=0.02, x=c=0.04, x=d=0.06, x=e=0.08, x=f=0.1)

3.4 SEM ANALYSIS

The SEM micrographs of all the samples of the series $Ti_{0.9}Co_{0.1-x}Cr_xO_2$ are shown in fig.4.These micrographs depict clear tetragonal picture with well defined boundaries. It can be seen that surface morphology is homogenous without any agglomerates. From these graphs Grain sizes were measured by linear line fit method whose values are given in Table 1.

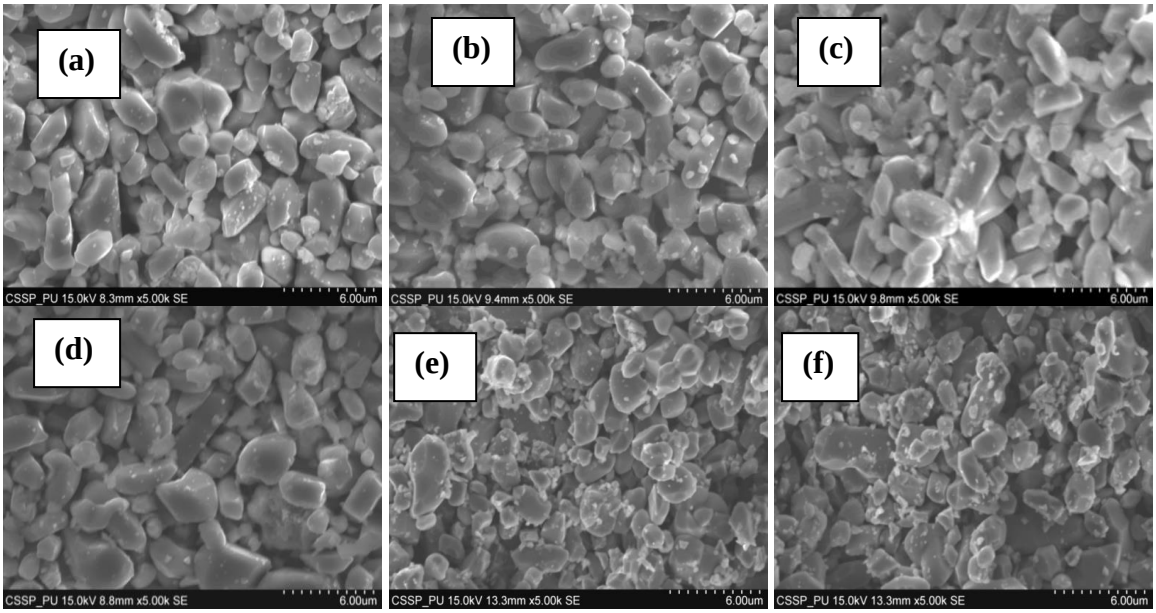

Fig 4. SEM micrographs of $Ti_{0.9}Co_{0.1-x}Cr_xO_2$ (x=a=0.0, x=b=0.02,x=c=0.04, x=d=0.06, x=e=0.08, x=f=0.1)

3.5 VSM Analysis

Hysteresis loops of the series $Ti_{0.9}Co_{0.1-x}Cr_xO_2$ are shown in Fig. 5. However all the samples showed Paramagnetic behavior and none of the samples showed ferromagnetic behavior at room temperature. This might be due to the fact that predominant Co spins are uncoupled at room temperature [21]. This Paramagnetic behavior of TiO_2 with Co at room temperature has also been observed by Baunie et al. He observed that ferromagnetism can be induced in single crystal of Rutile in oxygen deficient environment. When Cr which is antiferromagnetic in nature is added to TiO_2-Co system, it appears to be paramagnetic. The behavior of Cr in TiO_2 based DMS towards magnetism is also not very good in case of bulk DMS. It has been reported that addition of Cr to rutile TiO_2 above a certain amount i.e. 6 atomic percent causes its paramagnetic behavior [8]. However in our case ferromagnetism did not appear even at amount below 6 atomic percent of Cr. When these magnetic dopants are added to TiO_2, they-did not show any ferromagnetic behavior. The absence of Ferromagnetism in these samples at room temperature indicates the strong antiferromagnetic interactions among magnetic ions [22].These results are contrary to earlier experimental findings. [23]

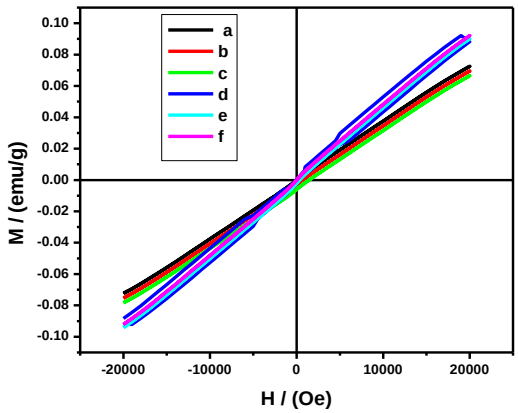

Fig 5. Hysteresis loops of $Ti_{0.9}Co_{0.1-x}Cr_xO_2$ (x=a=0.0, x=b=0.02, x=c=0.04, x=d=0.06, x=e=0.08, x=f=0.1)

3.6 UV-Visible Analysis

The band gap energy E_g versus $(\alpha h\nu)^2$ plots of series $Ti_{0.9}Co_{0.1-x}Cr_xO_2$ is shown in Fig.6 (a, b). Band gap energy E_g is determined by Tauc's equation [22] given as

$$\alpha (h\nu) = A (h\nu - E_g)^m \quad (4)$$

Where α is the absorption coefficient, hν is the photon energy, E_g is band gap energy and A is a constant known as band tailing parameter which is different for different material. The magnitude of m is characteristic of the type of transition and takes the value ½, 3/2, 2 and 3 for direct, allowed forbidden, indirect allowed and indirect forbidden transitions, respectively. The linear part of the curves is extrapolated to α=0 to get direct band gap energy. It is observed that band gap energy (E_g) decreases as the concentration of Cr increases. It is due to the fact that as Co and Cr are added to a TiO_2, impurity band is generated within the band gap. Electrons in the valence band absorb high energy photon and transfer to the impurity band (higher energy state) then secondary transfer from the impurity band to the conduction band by absorbing other photons. Optical absorption of metal semiconductor depends on this impurity band. Moreover the red shift developed here can be attributed to charge transitions between metal ion d electrons and the valence or conduction band of TiO_2. These results are in agreement with the earlier experimental studies [24].

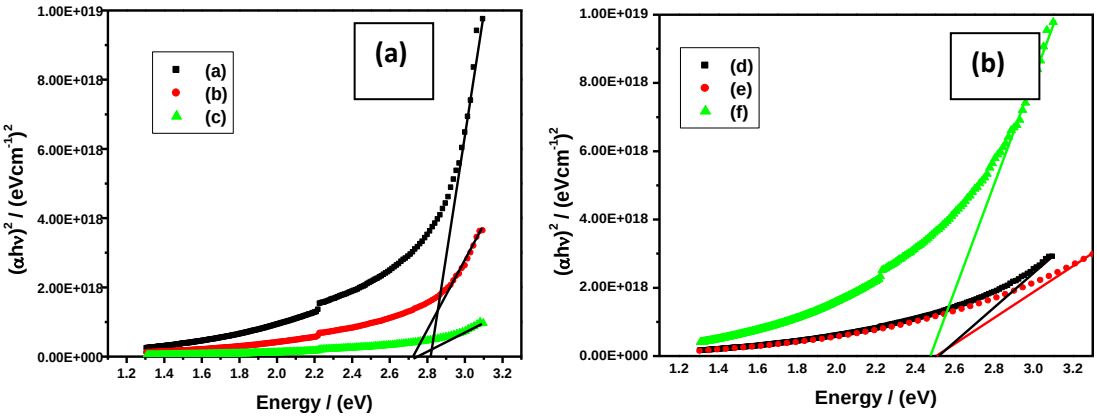

Fig 6. Band gap energy of $Ti_{0.9}Co_{0.1-x}Cr_xO_2$ (a) x=a=0.0, x =b= 0.02, x=c= 0.04 (b) x=d=0.06, x=e= 0.08, x=f=0.1

3.7 Electrical Resistivity Measurement

Fig.7. shows the plot of volume resistivity ρ_v as a function of temperature. 'ρ_v' was measured using the relation

$$\rho_v = R_vA/L \quad (5)$$

Where ρ_v is volume resistivity, Rv' the measured volume resistance, 'A' the total area of the samples (in pellets form) and 'L' is the thickness of the pellet across which the volume resistance had been measured. The overall trend of the curves is that the DC electrical resistivity value decreases with the rise of temperature confirming the semiconductor nature of material [25].
This decrease in resistivity is also observed by four probe technique at room temperature. The values of resistivity are given in Table 1.

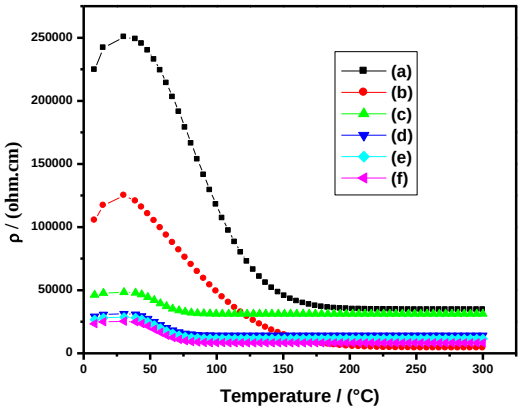

Fig7. Resistivity as a function of temperature of $Ti_{0.9}Co_{0.1-x}Cr_xO_2$ (x=a=0.0, x =b= 0.02, x=c= 0.04 x=d=0.06, x=e= 0.08, x=f=0.1)

4. Conclusions

An attempt has been made to fabricate $Ti_{0.9}Co_{0.1-x}Cr_xO_2$ based DMS by Powder metallurgy route. Structural properties have confirmed the formation of rutile phase of TiO_2. Magnetic measurements at room temperature showed absence of ferromagnetism for all Cr concentrations. The prepared series of $Ti_{0.9}Co_{0.1-x}Cr_xO_2$ lie in semiconducting range which has been confirmed by resistivity measurements and U-V Visible analysis. Our results have revealed that prepared series of $Ti_{0.9}Co_{0.1-x}Cr_xO_2$ is a Paramagnetic DMS.

Acknowledgement

The authors would like to thank Dr Hafza Khusrhid, University of South Florida Tampa Florida, USA, for her technical support.

References

[1] Q. Wang, X. Liu, X. Wei , J. Dai , W. Li, J. Nanomaterials **2015**, 1 (2015).
[2] S. Kirit and S. Dimple J. Crystal Growth **352**, 224, (2012).
[3] M. Taskin, J. Podder, App. Science Report 2(3), 107 (2014).
[4] B. Choudhury and A. Choudhury, Curr. Applied Physics **13**, 1025 (2013).
[5] A. Bouaine, G. Schmerber, D. Ihiawakrim, A. Derory, Mater.Science and.Engineering B **177**, 1618 (2012)
[6] C. Silva , A.R.G Costa , R.C DaSilva , L.C Alves , L.P Ferreira , M.D Carvalho, Franco N , M Godinho, M.M Cruz, J. Magnetism and Magnetic Materials **364**, 106 (2014).
[7] J. Tian , H. Gao , H. Deng , L. Sun , H. Kong , Yang P and Chu J. Alloys and Compounds **581**, 318 (2013).
[8] S Koohpayeh , A Williams , J Abell , J Lim, E Blackburn , J. Applied Physics **108**, 073919 (2010).
[9] M Chakrabarti, D Dechoudhury , T Senyal , K Roy , D Bhowmick, A Chakrabarti J. Physics.D **41**, 135006(2008)
[10] S. Mehraj, M.S. Ansari , Alimuddin , Physica E **65**, 84 (2015).
[11] X. Ping , L. Lan , Y. Li, Z. Xiao-Song , C. Xi-Ming, W.Jian-Feng, Z. Feng-Ming , Z. Wei , D. You-Wei , Chin. Physics Letter **26**, 097502 (2009).
[12] P Xu, L Li , L-Y Lv , Z X Song, C X Ming, W J Feng, Z Feng Ming , Z Wei , Y. Weild ,

Chin. Physics Letter, **26**, 097502 (2009).
[13] R.D. Shannon, Acta. Crystal A32, 751(1976).
[14] S. Anjum, H.M Tahir, K. Hussain, M. Rehman, M.S Rafique, S. Naseem , Physica B, **406,** 2555 (2012).
[15] H. Wang, J. Wei, R. Xiong , J. Shi , J. Magnetism and Magnetic Materials, **324**, 2057 (2012).
[16] F.D.Hardcastle, J. Arkansas Academy of Science **65**, 43 (2011).
[17] O. Toshiaki, I Fujio, F Yoshinori, J. raman spectroscopy **7**, 321(1978).
[18] A. H. Mayabadi , V. S. Waman , M. M. Kamble, S. S. Ghosh , B. B. Gabhale , S. R. Rondiya A.V. Rokade, S. S. Khadtare, V. G. Sathe, H. M. Pathan, S. W. Gosavi , S. R. Jadkar J. Physics and Chemistry of Solids **15**, 1 (2013).
[19] S. K. Gupta, J. Singha, K. Anbalagan , P. Kothari , R. R. Bhatia, P. K. Mishra, V. Manjuladevi , R. K. Gupta and J. Akhtar, Appl. Surface Science **264**, 737 (2013).
[20] Marc de grefend, Michael E .mchenry "structure of material: An introduction to crystallography, diffraction and symmetry" page 368.
[21] L. Mustafa , S. Anjum , S. Waseem , R. Zia, R Choudhry , S. M. Ramay , A Mahmood, S. Atiq, S. Khan , Adv Condense **M**atter Physics **2014**, 1 (2014).
[22] D. Chu , P. Zeng , D. Jiang, Y. Masuda, Sci. Advance Materials **1** , 227 (2009).
[23] J. Tauc , R. Grigorovici , A. Vancu, Phys.Status solidi **15**, 627 (1966).
[24] T. Sun , J. Fan , E. Liu , L. Liu , Y. Wang , H. Dai , Y. Yang , W. Hou , X. Hu , Z. Jiang , Powder Technology **228**, 210 (2012).
[25] M .Saleem, Preparation and Characterization of ZnO based Diluted Magnetic Semiconductor Materials (Ph.D. Dissertation). University of Punjab, Lahore (2013).